

# Magnetically sensitive light-induced reactions in cryptochrome are consistent with its proposed role as a magnetoreceptor

Kiminori Maeda<sup>a,1</sup>, Alexander J. Robinson<sup>a,1</sup>, Kevin B. Henbest<sup>a</sup>, Hannah J. Hogben<sup>b</sup>, Till Biskup<sup>b</sup>, Margaret Ahmad<sup>c,d</sup>, Erik Schleicher<sup>e</sup>, Stefan Weber<sup>e</sup>, Christiane R. Timmel<sup>a,2</sup>, and P. J. Hore<sup>b,2</sup>

<sup>a</sup>Department of Chemistry, University of Oxford, Centre for Advanced Electron Spin Resonance, Inorganic Chemistry Laboratory, Oxford OX1 3QR, United Kingdom; <sup>b</sup>Department of Chemistry, University of Oxford, Physical and Theoretical Chemistry Laboratory, Oxford OX1 3QZ, United Kingdom; <sup>c</sup>Université Paris VI, 4 Place Jussieu, 75005 Paris, France; <sup>d</sup>Pennsylvania State University, Media, PA 19063; and <sup>e</sup>Institute of Physical Chemistry, Albert-Ludwigs-Universität Freiburg, 79104 Freiburg, Germany

Edited by\* Nicholas J. Turro, Columbia University, New York, NY, and approved January 27, 2012 (received for review November 17, 2011)

Among the biological phenomena that fall within the emerging field of “quantum biology” is the suggestion that magnetically sensitive chemical reactions are responsible for the magnetic compass of migratory birds. It has been proposed that transient radical pairs are formed by photo-induced electron transfer reactions in cryptochrome proteins and that their coherent spin dynamics are influenced by the geomagnetic field leading to changes in the quantum yield of the signaling state of the protein. Despite a variety of supporting evidence, it is still not clear whether cryptochromes have the properties required to respond to magnetic interactions orders of magnitude weaker than the thermal energy,  $k_B T$ . Here we demonstrate that the kinetics and quantum yields of photo-induced flavin—tryptophan radical pairs in cryptochrome are indeed magnetically sensitive. The mechanistic origin of the magnetic field effect is clarified, its dependence on the strength of the magnetic field measured, and the rates of relevant spin-dependent, spin-independent, and spin-decoherence processes determined. We argue that cryptochrome is fit for purpose as a chemical magnetoreceptor.

magnetic compass | magnetoreception | migratory birds | quantum biology | radical pair mechanism

Originally identified in plants (1), and subsequently found in organisms ranging from bacteria to insects and mammals, cryptochromes are blue-light photoreceptor proteins with a variety of functions including entrainment of circadian rhythms and, in plants, light-dependent regulation of growth and development [reviewed in Ref. (2)]. They have high sequence-homology and structural similarity to their evolutionary ancestors, the DNA photolyases (3, 4) and all members of the cryptochrome/photolyase family contain the redox-active cofactor flavin adenine dinucleotide (FAD). Cryptochromes were proposed as potential magnetoreceptors by Ritz et al. in 2000 in an attempt to explain the mechanism by which migratory birds are able to sense the direction of the Earth’s magnetic field for the purpose of navigation (5). Based on an earlier suggestion by Schulten (6), and drawing on the known magnetic sensitivity of radical-pair reactions in vitro [reviewed in Ref. (7)], this idea has gained considerable support. Eleven years after the original suggestion, cryptochrome remains the only candidate radical-pair magnetoreceptor.

Photoreduction of the fully oxidized state of FAD in most proteins of the cryptochrome/photolyase family appears to be mediated by electron transfer along a conserved triad of tryptophan (Trp) residues to give a flavosemiquinone radical,  $FAD^{\bullet-}$  or  $FADH^{\bullet}$ , together with a radical derived from the terminal residue of the Trp-triad (8–11) (Fig. 1). At least in plants, where the photo-active functions of cryptochromes are best understood, the flavosemiquinone form of the protein is thought to be the signaling state (12, 13). If the quantum yield of this state were dependent on the direction of the Earth’s magnetic field, then in principle cryptochrome could act as a compass sensor. The evidence

accumulated over the last 11 years in support of the cryptochrome hypothesis has been reviewed in Refs. (14, 15). Hitherto, cryptochrome photochemistry has not been shown to be magnetically sensitive.

Cryptochromes have also attracted attention as potential mediators of biological effects of extremely low frequency (ELF) electromagnetic fields. Five observations are pertinent here. (i) Epidemiology suggests a weak association between increased risks of childhood leukemia and long-term exposure to 50/60 Hz ELF fields stronger than 0.4  $\mu T$  (16, 17). On this evidence, the International Agency for Research on Cancer (a part of the World Health Organization) has classified ELF magnetic fields as “possibly carcinogenic to humans” (18). The UK National Radiological Protection Board (now the Health Protection Agency), however, concluded in 2001 that there was no compelling evidence for carcinogenicity (19). (ii) Disruption of circadian timing has been associated with susceptibility to cancer (20). (iii) Cryptochromes are key components in the transcriptional regulation of mammalian circadian clocks (although there is no evidence that they function as photoreceptors or for the involvement of radicals) (2). (iv) The radical-pair mechanism is currently the only physically plausible mechanism by which magnetic interactions that are orders of magnitude weaker than  $k_B T$  can affect chemical reactions (7, 21). (v) Of the various radical-pair systems considered as possible mediators of biological magnetic-field effects, cryptochromes are the most likely candidates given their known (photo-)chemical and physical properties (22).

In the following, we demonstrate that photo-induced radical pairs in a cryptochrome (Cry-1 from the plant *Arabidopsis thaliana*, *AtCry*) are sensitive in vitro to weak applied magnetic fields. Comparing the behavior of *AtCry* with that of *Escherichia coli* photolyase (*EcPL*), we determine the reaction steps responsible for the magnetic-field effect, elucidate what appears to be the principal spin-decoherence mechanism, obtain estimates of the rates of these processes, and provide evidence that radical pairs in cryptochromes could have the properties required to respond to Earth-strength (approximately 50  $\mu T$ ) fields at physiological temperatures.

Author contributions: C.R.T. and P.J.H. designed research; K.M., A.J.R., and K.B.H. performed research; K.M., A.J.R., K.B.H., H.J.H., T.B., E.S., S.W., C.R.T., and P.J.H. discussed the data; M.A., E.S., and S.W. expressed the proteins; K.M., A.J.R., K.B.H., H.J.H., T.B., C.R.T., and P.J.H. analyzed data; and P.J.H. wrote the paper.

The authors declare no conflict of interest.

\*This Direct Submission article had a prearranged editor.

<sup>1</sup>These authors contributed equally to this work.

<sup>2</sup>To whom correspondence may be addressed. E-mail: peter.hore@chem.ox.ac.uk or christiane.timmel@chem.ox.ac.uk.

This article contains supporting information online at [www.pnas.org/lookup/suppl/doi:10.1073/pnas.1118959109/-DCSupplemental](http://www.pnas.org/lookup/suppl/doi:10.1073/pnas.1118959109/-DCSupplemental).



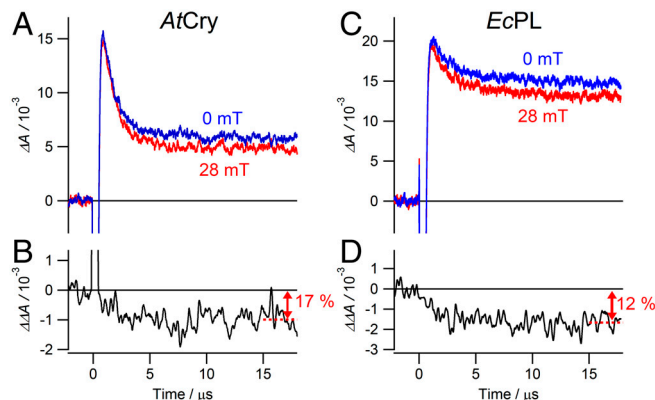


**Fig. 3.** Magnetic-field effects on the photochemical kinetics of AtCry and EcPL. Transient absorption kinetic time profiles of (A) AtCry and (C) EcPL both recorded at 510 nm with and without a 28 mT applied magnetic field. (B) and (D) Differences between the two signals shown in (A) and in (C), respectively:  $\Delta\Delta A = \Delta A(28 \text{ mT}) - \Delta A(0)$ . 200 ns boxcar smoothing was used to produce (B) and (D); no smoothing was used for (A) and (C). Experimental conditions: AtCry, 270 K in 60% (v/v) glycerol solution; EcPL, 250 K in 50% (v/v) glycerol solution. Similar traces for both proteins were observed at temperatures between 240 K and 275 K and glycerol contents between 25% and 65% (SI Appendix).

in Fig. 4. RP1 interconverts coherently between singlet and triplet states under the influence of magnetic interactions internal to the radicals (electron-nuclear hyperfine couplings) and Zeeman interactions with the external magnetic field. Only the singlet state of RP1 can revert to the ground state (FAD + TrpH) by electron-hole recombination, the corresponding reaction of the triplet state being spin-forbidden. Simultaneously, one of the constituents of RP1 changes its protonation state to give RP2, a process that is not subject to spin-selection rules and which singlet and triplet undergo at equal rates. The applied magnetic field alters the time-dependent probability that RP1 is singlet or triplet and so changes the fractions of radical pairs that proceed along the two competing pathways. The nonequilibrium state of the spin system allows magnetic interactions much weaker than  $k_B T$  to alter the reaction yields. As indicated by the transient absorption data (Figs. 2 and 3), the RP1 reactions occur on a 10  $\mu$ s timescale; i.e., slow enough to allow time for a 50  $\mu$ T magnetic field to modify the singlet-triplet interconversion and fast enough to compete with spin-decoherence, which has been shown by time-resolved EPR to occur in approximately 10  $\mu$ s (11). Experi-

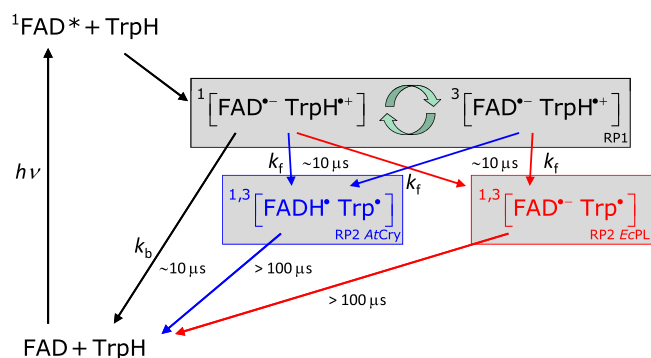


**Fig. 4.** Proposed photochemical reaction schemes for AtCry and EcPL. The black arrows and species are common to both proteins; the blue and red features refer to AtCry and EcPL, respectively.  $k_b$  and  $k_f$  are first-order rate constants for electron-hole recombination of RP1 and formation of RP2 from RP1, respectively. Although RP2 in AtCry is here drawn as [FADH•Trp•], the protonation state of the Trp radical is not certain. The curved green arrows indicate the coherent, magnetic field-dependent interconversion of the singlet and triplet states of RP1.

mental evidence that RP1 is formed in a *singlet* state from the photo-excited singlet state of the FAD cofactor ( $^1\text{FAD}^*$ ) is discussed in the [SI Appendix](#).

**Kinetic Regulation of Magnetic Responses.** The changes in the photochemical kinetics of *AtCry* and *EcPL* reported above are produced by applied magnetic fields some 500 times stronger than the Earth's field. To shed light on the conditions under which cryptochrome might be sensitive to much weaker fields, we have sought to clarify some of the factors that determine the amplitude of the responses at 28 mT.

A 28 mT magnetic field elicits 10–20% changes in the yield of RP2 in both *AtCry* and *EcPL* (Fig. 3), substantially larger than the 3–4% effects previously reported for *EcPL* in a solution with a lower glycerol content (23). A possible explanation for this difference can be found in the earlier observation (30) that the deprotonation rate ( $k_f$ ) of the terminal  $\text{TrpH}^{\bullet+}$  radical in *EcPL* decreases with increasing concentration of glycerol, an effect attributed to release of the proton to the solvent. Changes in  $k_f$  alter the competition between the  $k_b$  and  $k_f$  reactions (Fig. 4) and so have the potential to tune the magnetic-field effect. As shown in Fig. 5 for *EcPL*, both the lifetime of RP1 (determined by the  $k_b$  and  $k_f$  steps, Fig. 4) and the magnetic-field effect on the quantum yield of RP2 increase with increasing glycerol concentration and decreasing temperature, with an approximately linear correlation between the two quantities. We comment on the origin of this effect in the [SI Appendix](#).

**Magnetic-field Dependence of Radical Yields.** Effects of magnetic fields substantially weaker than 28 mT have been explored for *AtCry* and *EcPL*; the results are shown in Fig. 6. The fractional change in the yield of RP2 (as measured at 510 nm) is given for magnetic fields down to about 1 mT. The changes are roughly three times stronger for *AtCry* than for *EcPL* but otherwise rather similar. Above 5 mT, both proteins show typical radical-pair behavior (7): a monotonic increase in the magnitude of the effect, leveling off in both cases at magnetic fields stronger than about 25 mT. The comparatively large asymptotic magnetic-field effects (>20% for *AtCry* and >8% for *EcPL*) observed here are assumed to arise from the relatively long lifetime of the protein-bound radicals and the restrictions placed on their dynamics by the protein environment.

The width of such field-profiles is often characterized by the parameter  $B_{\frac{1}{2}}$ , the magnetic field at which the effect reaches half

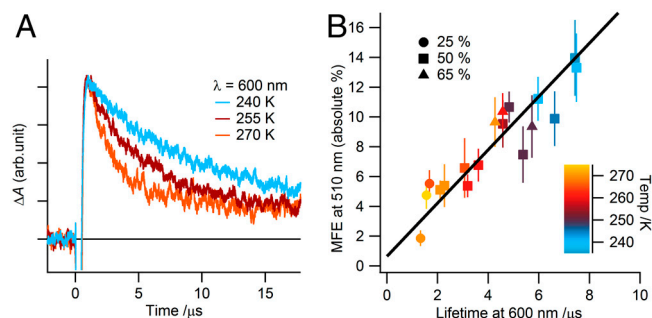


**Fig. 5.** Correlation between the magnetic-field effect on the yield of RP2 and the lifetime of RP1 in *EcPL*. (A) Transient absorption kinetic time profiles of *EcPL* in 50% (v/v) glycerol solution in the absence of an applied magnetic field at the temperatures indicated. Recorded at 600 nm, these signals reflect the kinetics of the reactions:  $\text{TrpH}^{*+} \rightarrow \text{Trp}^* + \text{H}^+$  and  $[\text{FAD}^{*-}\text{TrpH}^{*+}] \rightarrow \text{FAD} + \text{TrpH}$  (Fig. 4). Lifetimes were extracted from such data by fitting to a monoexponential decay with a constant offset. (B) Effect of a 28 mT magnetic field on the yield of RP2 (recorded at 510 nm) plotted against the lifetime of RP1 (measured at 600 nm) over a range of temperatures and glycerol concentrations, as indicated. The vertical axis is the absolute value of the fractional magnetic-field effect (MFE):  $|\Delta A(28 \text{ mT}) - \Delta A(0)|/\Delta A(0)$ . The data plotted here are given in the [SI Appendix](#).



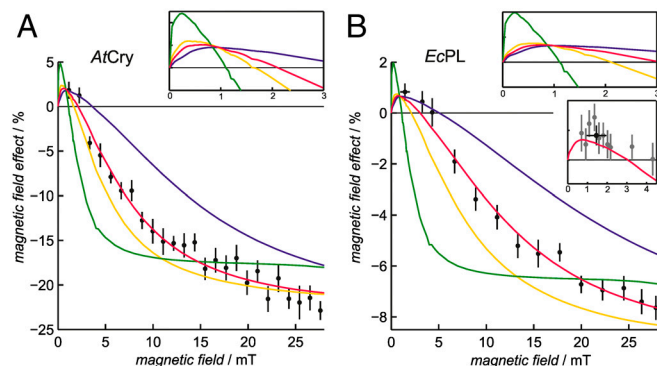
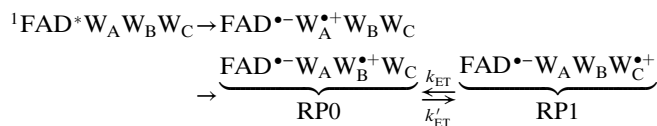


**Fig. 6.** Magnetic field-dependence of the yield of RP2 in AtCry and EcPL. The percentage change in the yield of RP2 (measured at 510 nm) as a function of the strength of the applied magnetic field for (A) AtCry and (B) EcPL. Experimental conditions: (A) AtCry, 60% glycerol, 270 K; (B) EcPL, 50% glycerol, 260 K. The red lines are the best-fit simulations obtained using the singlet-triplet dephasing model described in the text, with  $k_f = 2.5 \times 10^5 \text{ s}^{-1}$  and (A)  $k_b = 4.9 \times 10^5 \text{ s}^{-1}$ ,  $k_{STD} = 1.1 \times 10^7 \text{ s}^{-1}$ ; (B)  $k_b = 1.2 \times 10^5 \text{ s}^{-1}$ ,  $k_{STD} = 2.7 \times 10^7 \text{ s}^{-1}$ . The other lines are simulations with the same values of  $k_f$  and  $k_b$  but (A)  $k_{STD}/\text{s}^{-1} = 0$  (green),  $5 \times 10^6$  (yellow),  $5 \times 10^7$  (blue); (B)  $k_{STD}/\text{s}^{-1} = 0$  (green),  $1 \times 10^7$  (yellow),  $1 \times 10^8$  (blue). The two larger insets show expanded views of the simulations in the low field region. The irregularities visible in some of these curves arise from energy-level anticrossings. The smaller inset in (B) shows, on an expanded scale, the best-fit simulation together with 8 measurements in the range 0.7–2.2 mT that were averaged to obtain the (black) point plotted at  $B = 1.5$  mT in this inset and in the main panel. The error bars associated with this data point represent  $\pm$  one standard deviation of the eight measurements. Each data point in the main panels is the average of (A) 10 and (B) 40 ( $>3$  mT) or 80 ( $<3$  mT) transients. At each applied magnetic-field strength  $B$ , the double-difference kinetic time profiles  $\Delta A(B) - \Delta A(0)$  were smoothed with (A) 5  $\mu\text{s}$  and (B) 0.5  $\mu\text{s}$  boxcar functions. The mean  $\pm$  standard deviation (calculated over the time intervals: (A) 2–170  $\mu\text{s}$  and (B) 7–15  $\mu\text{s}$ ) is plotted for each datum.

its limiting size at high field. Using hyperfine coupling data for  $\text{FAD}^{\bullet-}$  and  $\text{TrpH}^{\bullet+}$ , the Weller equation (31) gives an estimate for  $B_{\frac{1}{2}}$  of approximately 3 mT for RP1 (see *SI Appendix*). The observed values of  $B_{\frac{1}{2}}$  (Fig. 6) are substantially larger: around 10–12 mT for both proteins. Discrepancies of this kind occur quite commonly for radical-pair reactions and have often been attributed to electron spin-decoherence within the radical pair (see below) (32, 33). Also visible in Fig. 6 are indications that for both proteins the phase of the magnetic response inverts for magnetic fields weaker than 2–3 mT. We return to this point below.

**Reversible Electron Transfer in the Trp Triad.** The theoretical basis of the radical-pair mechanism is sufficiently developed that quantitative interpretation of experimental data has become fairly routine especially when, as here, the separation and relative orientation of the two radicals are constrained. Even though the data in Fig. 6 exhibit little structure, successful numerical simulations may supply insights into the decoherence mechanism(s) responsible for the larger than expected  $B_{\frac{1}{2}}$  values.

Reversible electron transfer between the distal and intermediate residues of the Trp triad has the potential to increase the observed  $B_{\frac{1}{2}}$ . Denoting the proximal, intermediate and distal tryptophans as  $W_A$ ,  $W_B$ , and  $W_C$ , the electron transport chain may be written:



where  $k_{ET}$  and  $k'_{ET}$  are the rate constants for interconversion of RP1 and the intermediate radical pair comprising  $\text{FAD}^{\bullet-}$  and

$W_B^{\bullet+}$ , which we shall call RP0. The limited evidence available suggests that the Trp radical is mostly localized on  $W_C$  (i.e.,  $k_{ET} \gg k'_{ET}$ ) and that  $k'_{ET}$  may be fast enough to allow reversible electron hopping from and to  $W_B$  during the lifetime of RP1 (26, 34, 35). Using center-to-center FAD-Trp separations calculated (36) from the X-ray structure of AtCry (37) (1.32 nm for RP0 and 1.90 nm for RP1), the interradical electron exchange interactions have been estimated (36) as  $|J_{RP0}| \approx 10^3 \text{ mT}$  and  $|J_{RP1}| \approx 10^{-1} \text{ mT}$ . Since  $|J_{RP0}|$  greatly exceeds  $|J_{RP1}|$ , the hyperfine interactions and the magnetic-field strength, electron hopping would cause strong modulation of the exchange interaction resulting in rapid relaxation of singlet-triplet coherences in RP1 (33). The time required for such decoherence is on the order of  $(J_{RP0})^{-1}$ ; i.e., approximately 10 ps. Therefore, if  $k_{ET}$  is not much larger than  $10^{11} \text{ s}^{-1}$ , every time RP1 is converted into RP0 there would be significant decoherence before the electron jumped back. Under these conditions, the singlet-triplet dephasing (STD) rate,  $k_{STD}$ , should be close to  $k'_{ET}$ .

Standard techniques of quantum spin dynamics (7) were employed to simulate the magnetic-field effects shown in Fig. 6, using the reaction scheme in Fig. 4. Just two (field-independent) variable parameters were used for each protein:  $k_b$  and  $k_{STD}$ . The rate constant for the  $\text{RP1} \rightarrow \text{RP2}$  reaction was fixed ( $k_f = 2.5 \times 10^5 \text{ s}^{-1}$ ) by noting that the magnetic-field effect for EcPL at 28 mT (approximately 8%, Fig. 6B) corresponds to a RP1 lifetime of approximately 4  $\mu\text{s}$  (Fig. 5B). The same value was used for AtCry. In the simulations, all coherent superpositions of a singlet state and a triplet state of RP1 were damped exponentially with the rate constant  $k_{STD}$ , and hyperfine couplings were calculated using density functional theory. The red lines in Figs. 6A and B are the best-fit simulations, with the optimum parameter values: AtCry,  $k_b = 4.9 \times 10^5 \text{ s}^{-1}$ ,  $k_{STD} = 1.1 \times 10^7 \text{ s}^{-1}$ ; EcPL,  $k_b = 1.2 \times 10^5 \text{ s}^{-1}$ ,  $k_{STD} = 2.7 \times 10^7 \text{ s}^{-1}$ . These numbers are plausible: (i) A magnetic-field effect as large as approximately 20% requires effective competition between the two reaction pathways, implying  $k_b \approx k_f$ . (ii) RP1 lifetimes with respect to recombination to the ground state (i.e.,  $k_b^{-1}$ ) of approximately 2  $\mu\text{s}$  (AtCry) and 8  $\mu\text{s}$  (EcPL) are compatible with the observed transient absorption kinetics. (iii) As shown in Fig. 6, the width of the field-dependence is sensitive to the value of  $k_{STD}$ ; an increase in  $B_{\frac{1}{2}}$  from approximately 3 mT to 10–12 mT requires  $k_{STD}$  to be substantially larger than  $k_b$  and  $k_f$ . (iv) The value of  $k_{STD}$  for EcPL agrees very well with the estimate of  $k'_{ET}$  by Popović et al. ( $3.2 \times 10^7 \text{ s}^{-1}$ ) (26) but less well with that of Krapf et al. ( $1.2 \times 10^4 \text{ s}^{-1}$ ) (35). Simulations in which spin relaxation was omitted (*SI Appendix*), or included by means of other models, were uniformly unsuccessful in accounting for the data shown in Fig. 6 (see *SI Appendix* for details). Additional simulations, also described in the *SI Appendix*, suggest a rationale for the larger magnetic-field effect for AtCry compared to EcPL (Fig. 6) and for the correlation shown in Fig. 5.

**Sensitivity to Weaker Magnetic Fields.** We have shown that the effects of magnetic fields stronger than 5 mT are consistent with singlet-triplet interconversion induced by hyperfine and Zeeman interactions together with singlet-triplet dephasing brought about by electron hopping. In the light of this, we return to the sign change in the magnetic-field effect for both proteins below 2–3 mT (Fig. 6). Such phase inversions have been well documented both theoretically and experimentally in other reaction systems (21, 38, 39) and are usually referred to as “low field effects” (LFE). Numerical simulations of model radical pairs (21) show that when spin relaxation and radical recombination reactions are sufficiently slow, the LFE can be much larger than the 1% effects seen at around 1 mT in Fig. 6, even in much weaker magnetic fields. The best-fit simulations predict LFEs for both proteins with approximately the correct positions and amplitudes. The other simulations in Fig. 6 indicate that as  $k_{STD}$  is reduced

the initial slope increases causing the maximum LFE to shift to progressively lower fields. Thus the effect of a 50  $\mu$ T magnetic field on the yield of RP2 could be significantly larger than implied by the best-fit simulations in Fig. 6 if singlet-triplet dephasing (and any other significant decoherence mechanisms) were sufficiently slow.

## Discussion

The cryptochrome hypothesis of radical-pair magnetoreception was proposed 11 years ago. We present here direct evidence that cryptochromes can exhibit the magnetically sensitive photochemistry that is the essential prerequisite for a magnetic compass sensor. Magnetic-field effects on the quantum yields of radicals produced in *AtCry* in viscous solution of about +1% in a 1 mT magnetic field, and about -25% in a 30 mT field, have been detected. The change in phase observed for fields weaker than 2–3 mT is the signature of the low field effect which, under appropriate conditions, could permit significant responses to Earth-strength magnetic fields.

High glycerol concentrations and reduced temperatures have been used here to optimize the observed magnetic responses. One can only speculate about the environment of an avian cryptochrome in a magnetoreceptor cell, but it seems most likely that the proteins would have to be both immobilized and aligned in order to show the anisotropic magnetic responses essential for a compass detection mechanism (5). Restricted molecular motion, leading to slower spin-decoherence, should also be favorable. Both factors prompted our use of mixed aqueous solvents with a higher viscosity than pure water. [Other reasons for using glycerol-water mixtures were (i) to regulate the competition between deprotonation of  $\text{TrpH}^{*+}$  and spin-selective recombination of RP1 in *EcPL* (Fig. 5); (ii) to allow the use of temperatures below 273 K for the same reason; and (iii) to stabilize the protein against aggregation and precipitation.] Restricted motion could come about in different and probably more efficient ways in vivo, for example by tethering to membrane proteins or cytoskeletal filaments (40), binding to signaling partners (41–43) and/or cofactors [e.g., ATP (37, 44)], dimerization (45), etc. It does not seem unreasonable to conjecture that under optimum conditions in vivo, the effect of a 50  $\mu$ T magnetic field could be substantially larger than observed in the present study. Simulations suggest that the low field effect can, under the right conditions, be as large as 10–20% (21). Too little is known about light-dependent cryptochrome signaling in general, and magnetoreception in particular, to say whether this would be large enough to form the basis of a viable magnetoreceptor.

It is evident from our results that a significant magnetic-field effect from a cryptochrome-based radical pair requires kinetic competition on a 1–10  $\mu$ s timescale, between spin-selective electron-hole recombination, and spin-independent formation of the signaling state. If these processes were much faster than 1  $\mu$ s there would be insufficient time for the geomagnetic field to influence the spin dynamics; if they were much slower, the effect would almost certainly be attenuated by spin-decoherence (14). It seems unlikely, however, that the conformational changes needed to generate the signaling state [probably rearrangement of the C-terminal domain (46)] could be as fast as 10  $\mu$ s. Our results show that formation of a secondary species (RP2) from the magnetically sensitive radical pair RP1, [ $\text{FAD}^{*+}\text{TrpH}^{*+}$ ], avoids the need for an abnormally rapid protein rearrangement or exceptionally slow spin-decoherence. Protonation of the  $\text{FAD}^{*+}$  radical (as may occur in *AtCry*) or deprotonation of the  $\text{TrpH}^{*+}$  radical [as occurs in *EcPL* (23, 30)] allows the magnetic-field effect on RP1 to be “stored” in the form of a changed quantum yield of the

much longer lived state RP2, from which the signaling state can subsequently be generated. The fact that there is no need for the reactions of RP2 to be magnetically sensitive means that its lifetime can greatly exceed its spin-decoherence time without ill effect.

There are now two members of the cryptochrome/photolyase family that show magnetic responses. Given the very different biological functions of *EcPL* (DNA repair) and *AtCry* (regulation of growth and development, entrainment of circadian rhythms) and the fact that neither bacteria nor plants appear to have specialized magnetoreceptors, we suggest that magnetic sensitivity is a general feature of this protein family and that the results described here may be extrapolated to bird cryptochromes (and possibly even human cryptochromes).

## Materials and Methods

**Protein Preparation.** The expression and purification of *EcPL* (as a mutant that does not bind the methenyltetrahydrofolate cofactor) are described elsewhere (23, 47). To ensure the FAD cofactor was in its fully oxidized state, the protein was pretreated with potassium ferricyanide as described previously (23). Glycerol was added to approximately 130  $\mu$ M protein samples in 50 mM Hepes buffer at pH 7.0 with 100 mM KCl to obtain solutions containing 20–50% glycerol (v/v). Unlike our previous study of *EcPL* (23), potassium ferricyanide was not added to the samples to reoxidize photoreduced flavin.

*AtCry* (full length cryptochrome-1) was expressed in Sf21 cells using a recombinant baculovirus expression vector system and purified by Ni-NTA affinity chromatography. Glycerol was added to approximately 150  $\mu$ M protein samples in Tris/HCl buffer at pH 7.5 with 500 mM NaCl and 250 mM imidazole to obtain solutions containing 20–60% glycerol (v/v).

**Transient Absorption Spectroscopy.** Protein samples (approximately 250  $\mu$ L) were cooled in a cryostat (Oxford Instruments, Optistat CF) with the temperature controlled to within 0.1 K. The sample was held in a quartz cuvette (Hellma 104.002F QS; 10 mm path length, internal dimensions  $2 \times 10 \times 45$  mm) at the center of the cryostat. Magnetic-field pulses of approximately 4 ms duration, synchronized with the laser flash, were generated using home-built Helmholtz coils. The maximum magnetic field at the position of the sample was 29 mT. Samples were not shielded from the Earth's magnetic field. Radical pairs in *EcPL* and *AtCry* were generated by flash photolysis using a dye laser (Sirah Cobra) pumped by a Nd:YAG laser (Continuum Surelite 1). The laser dye was Coumarin 460 (Exciton Inc.) in analytical grade methanol (Fisher Scientific). The Nd:YAG laser produced 5 ns pulses with energy approximately 100 mJ and repetition rate 1 Hz, tuned by means of a Q-switch delay to produce 5–7 mJ, 460 nm pulses (FWHM 37 nm) from the dye laser. Probe light from a 300 W xenon arc lamp (Oriol) was passed through a water filter to cut out infrared components and through long-pass filters to remove unwanted wavelengths and then to the sample in a direction orthogonal to the pump pulses. Pump and probe beams were controlled by mechanical shutters to obtain a 0.05 Hz repetition rate to reduce photodegradation of the light-sensitive samples. Probe light was collected using a monochromator (Oriol 77250), fed into a photomultiplier tube (Hamamatsu R928) and from there to an oscilloscope (Iwatsu-LeCroy Waverunner LT342L). Data were transferred to a personal computer and analyzed using IGOR PRO (Wavemetrics, Inc.) software.

**Spin Dynamics Simulations.** The magnetic field-dependence of radical-pair reaction yields (Fig. 6) was calculated from the equation of motion of the radical-pair spin density operator in Liouville space including coherent spin dynamics, decoherence processes, and chemical reactivity by means of appropriate superoperators. Singlet-triplet dephasing was introduced as proposed by Shushin (33). Further details are given in the *SI Appendix*.

**ACKNOWLEDGMENTS.** We thank S. M. Lea, J. Lillington and A. Bowen for discussions and N. Baker and P. Stehle for technical assistance. P.J.H. and C.R.T. were supported by the Electromagnetic Fields Biological Research Trust, the Defense Advanced Research Projects Agency (QuBE: N66001-10-1-4061), and the Engineering and Physical Sciences Research Council. S.W. and E.S. were funded by Deutsche Forschungsgemeinschaft Grant WE2376/41.

1. Ahmad M, Cashmore AR (1993) *HY4* gene of *A. thaliana* encodes a protein with characteristics of a blue-light photoreceptor. *Nature* 366:162–166.
2. Chaves I, et al. (2011) The cryptochromes: Blue light photoreceptors in plants and animals. *Annu Rev Plant Biol* 62:335–364.

3. Weber S (2005) Light-driven enzymatic catalysis of DNA repair: A review of recent biophysical studies on photolyase. *Biochim Biophys Acta* 1707:1–23.
4. Sancar A (2008) Structure and function of photolyase and *in vivo* enzymology: 50th anniversary. *J Biol Chem* 283:32153–32157.



## SUPPORTING INFORMATION

### **Magnetically sensitive light-induced reactions in cryptochrome are consistent with its proposed role as a magnetoreceptor**

Kiminori Maeda<sup>a,1</sup>, Alexander J. Robinson<sup>a,1</sup>, Kevin B. Henbest<sup>a</sup>, Hannah J. Hogben<sup>b</sup>, Till Biskup<sup>b</sup>, Margaret Ahmad<sup>c</sup>, Erik Schleicher<sup>d</sup>, Stefan Weber<sup>d</sup>, Christiane R. Timmel<sup>a,2</sup> & P. J. Hore<sup>b,2</sup>

<sup>a</sup>Department of Chemistry, University of Oxford, Centre for Advanced Electron Spin Resonance, Inorganic Chemistry Laboratory, Oxford, UK.

<sup>b</sup>Department of Chemistry, University of Oxford, Physical & Theoretical Chemistry Laboratory, Oxford, UK.

<sup>c</sup>Université Paris VI, 4 Place Jussieu, 75005 Paris, France and Pennsylvania State University, Media, Pennsylvania 19063, USA.

<sup>d</sup>Institute of Physical Chemistry, Albert-Ludwigs-Universität Freiburg, 79104 Freiburg, Germany.

<sup>1</sup>These authors contributed equally to this work.

<sup>2</sup>To whom correspondence may be addressed. E-mail: peter.hore@chem.ox.ac.uk or christiane.timmel@chem.ox.ac.uk

### **Contents**

1. Magnetic field effects on radical kinetics
2. Flavin–tryptophan photoreaction mechanism
3. Correlation between the magnetic field effect on the yield of RP2 and the lifetime of RP1 in *EcPL*.
4. Calculation of  $B_{1/2}$
5. Simulation of magnetic field effects



## 1. Magnetic field effects on radical kinetics

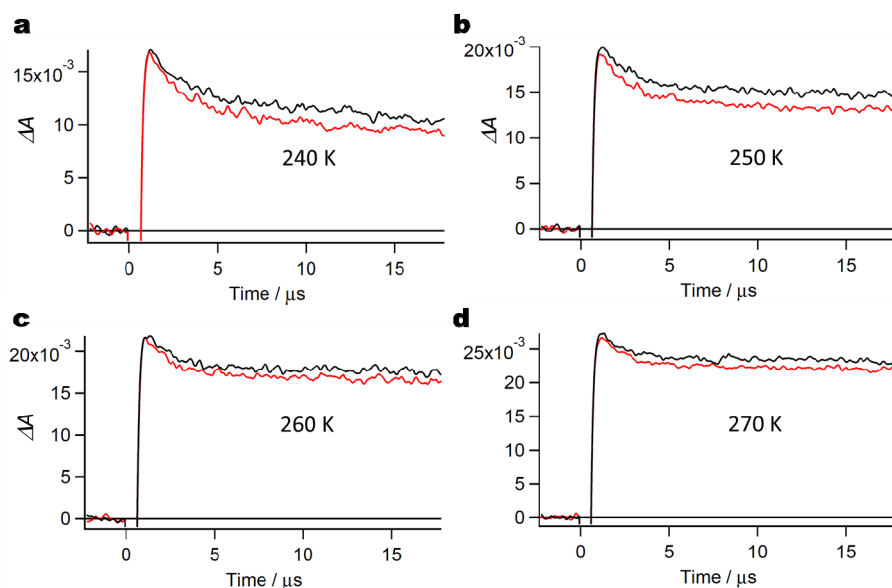


**Fig. S1.** Transient absorption kinetic time profiles of *EcPL* recorded at 510 nm in 50% glycerol solution with (red) and without (black) a 28 mT applied magnetic field at the temperatures indicated. Results were obtained as the average of 10 laser shots, with 200 ns boxcar smoothing.

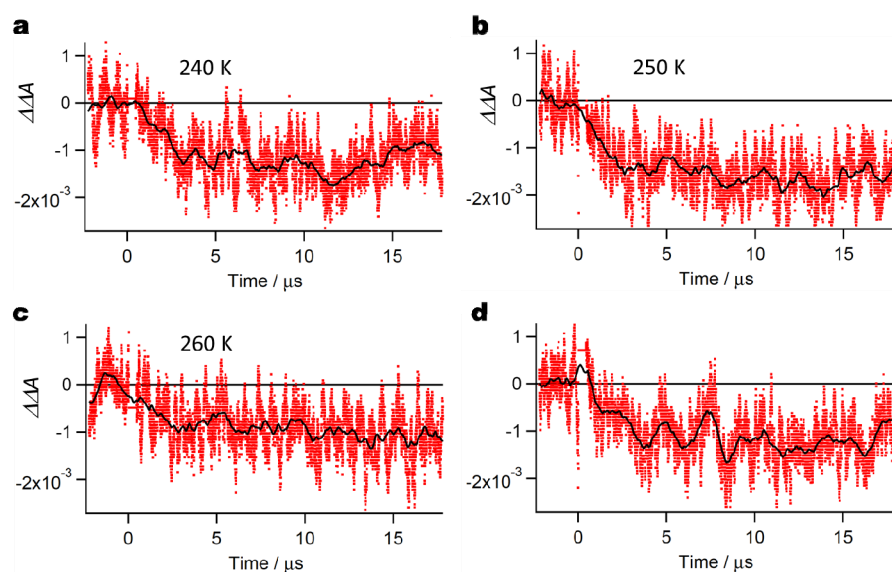


**Fig. S2.** Difference signals calculated from the data in Fig. S1:  $\Delta\Delta A = \Delta A(28 \text{ mT}) - \Delta A(0)$ . Red dots represent raw, unsmoothed data; black lines represent the same data after 1  $\mu\text{s}$  boxcar smoothing.



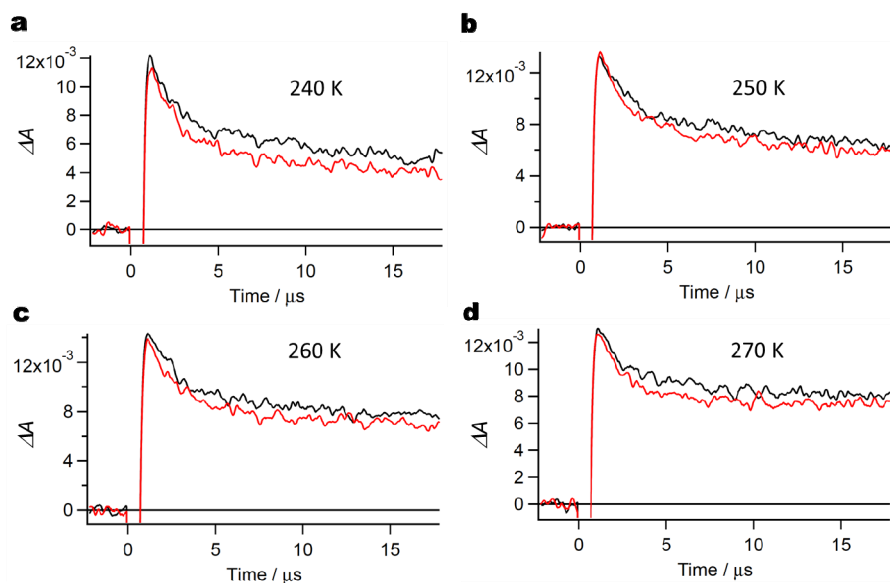


**Fig. S3.** Transient absorption kinetic time profiles of *EcPL* recorded at 510 nm in 65% glycerol solution with (red) and without (black) a 28 mT applied magnetic field at the temperatures indicated. Results were obtained as the average of 10 laser shots, with 200 ns boxcar smoothing.

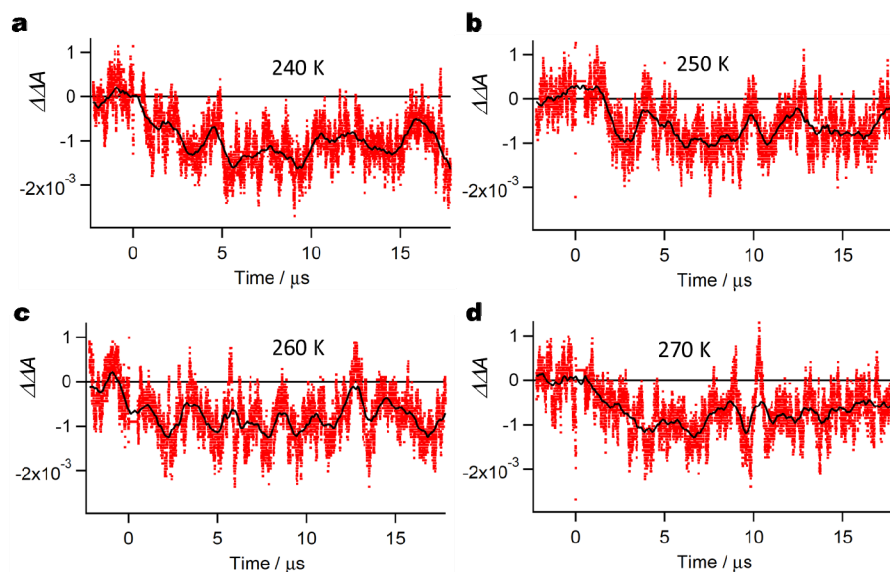


**Fig. S4.** Difference signals calculated from the data in Fig. S3:  $\Delta\Delta A = \Delta A(28 \text{ mT}) - \Delta A(0)$ . Red dots represent raw, unsmoothed data; black lines represent the same data after 1  $\mu\text{s}$  boxcar smoothing.

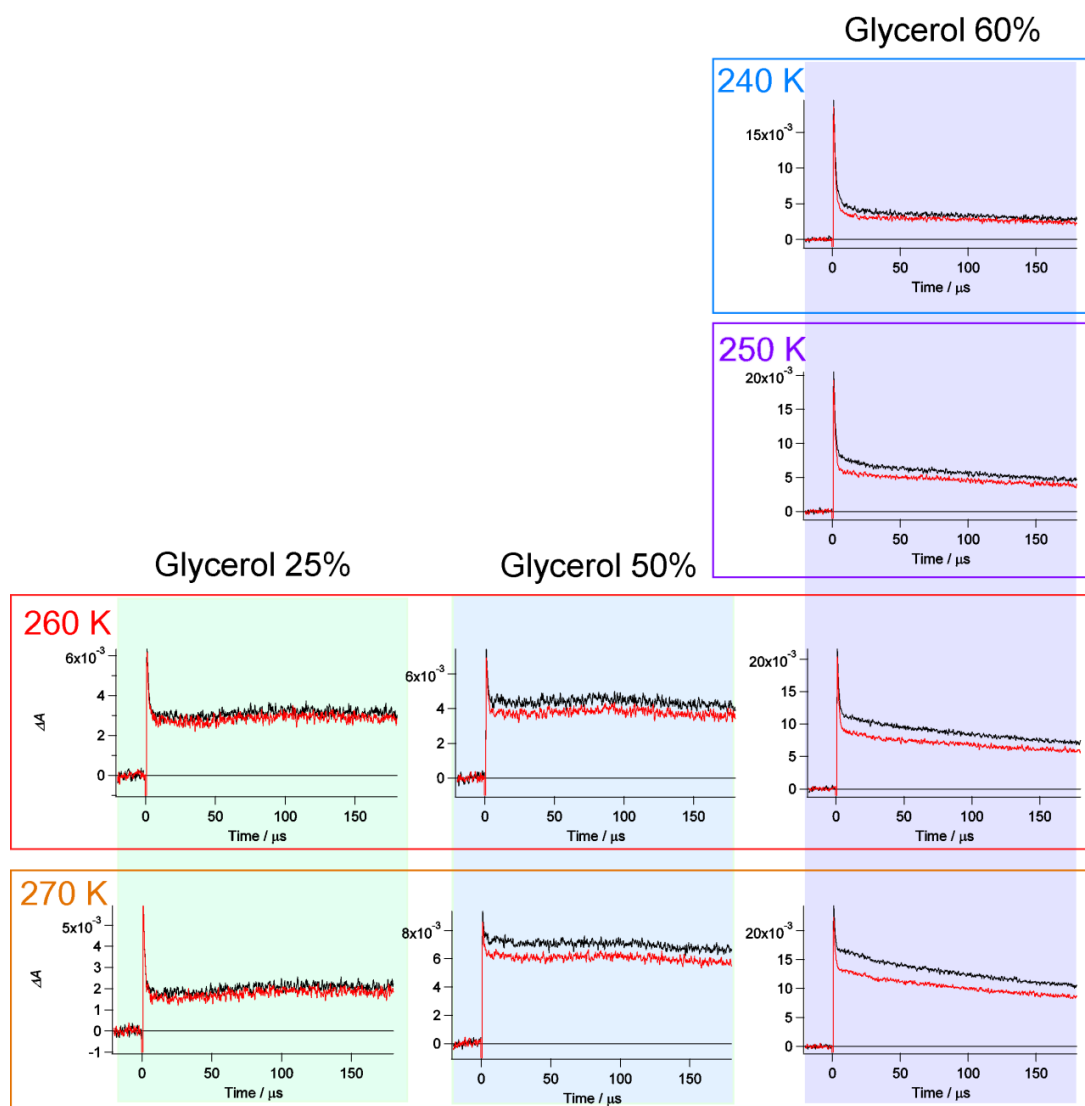


**Fig. S5.** Transient absorption kinetic time profiles of *AtCry* recorded at 510 nm in solutions of various water/glycerol composition and various temperatures with (red) and without (black) a 28 mT applied magnetic field. Results were obtained as the average of 10 laser shots, with 500 ns boxcar smoothing.

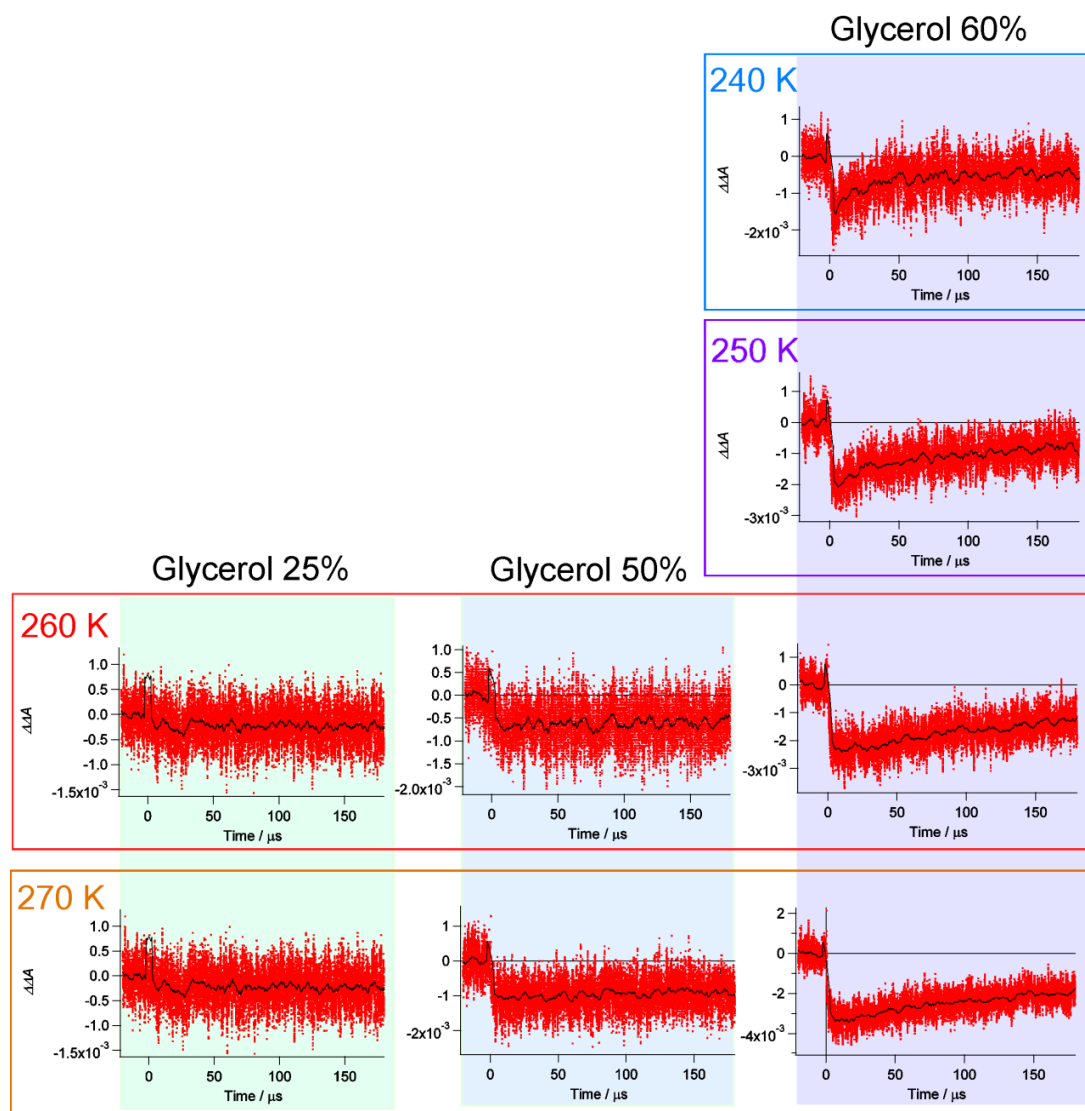


**Fig. S6.** Difference signals calculated from the data in Fig. S5:  $\Delta\Delta A = \Delta A(28 \text{ mT}) - \Delta A(0)$ . Red dots represent raw, unsmoothed data; black lines represent the same data after 5  $\mu\text{s}$  boxcar smoothing.

## 2. Flavin–tryptophan photoreaction mechanism

Fig. 4 shows RP1 as formed in a *singlet* state from the photo-excited singlet state of the FAD cofactor ( $^1\text{FAD}^*$ ) in AtCry and EcPL. Much of the photochemistry of free (i.e. not protein-bound) flavins proceeds from the photo-excited *triplet* state formed by intersystem crossing from the excited singlet. Although in principle possible in AtCry and EcPL, this reaction pathway is excluded by the observation that an applied magnetic field of intensity exceeding the hyperfine interactions *reduces* the yield of RP2 (Figs 2 and 3) and correspondingly *increases* the proportion of RP1 that returns directly to the ground state (1). Direct formation of RP1 from  $^1\text{FAD}^*$ , rather than via  $^3\text{FAD}^*$  probably has the advantage of a larger quantum yield because intersystem crossing is likely to be slower than electron transfer and so would compete less effectively with other processes that quench  $^1\text{FAD}^*$ , e.g. fluorescence.

The conclusion that electron transfer along the Trp-triad chain proceeds via a singlet route is supported by observations of magnetic field effects from flavin–tryptophan reaction systems that are known to proceed through the *triplet* route. Photo-induced electron transfer between a free flavin and surface-exposed tryptophan residues in hen egg white lysozyme (Fig. S7) and the apo-form of garden warbler Cry-1a (Fig. S8) show, as expected, magnetic field effects with the opposite phase, i.e. an *increased* yield of long-lived radicals. Formation of spin-correlated radical pairs via a *singlet* pathway in DASH-type cryptochromes has also been demonstrated using time-resolved EPR spectroscopy (2, 3).

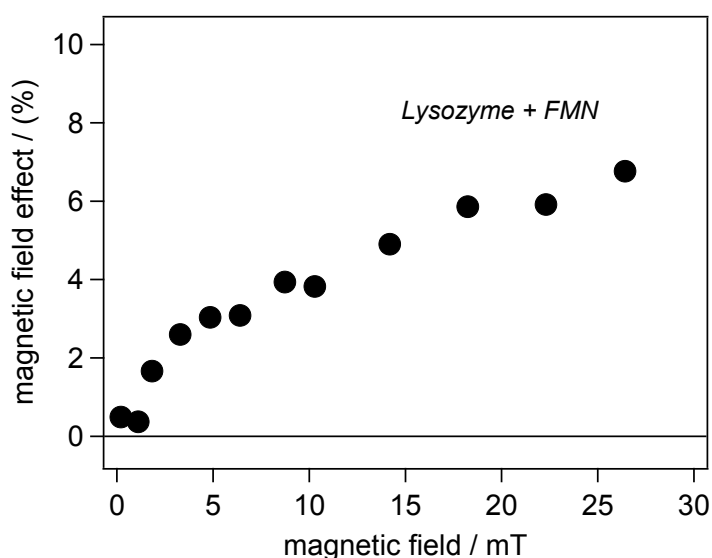


**Fig. S7.** Magnetic field effect on the yield of flavin mononucleotide (FMN) radicals formed by the intermolecular photochemical reaction of 200  $\mu\text{M}$  FMN with 500  $\mu\text{M}$  hen egg white lysozyme (data



reproduced from Ref (4)). The excited triplet state of the flavin undergoes electron transfer reactions with two solvent-exposed tryptophan residues (Trp-62 and Trp-123) on the surface of the protein (5).

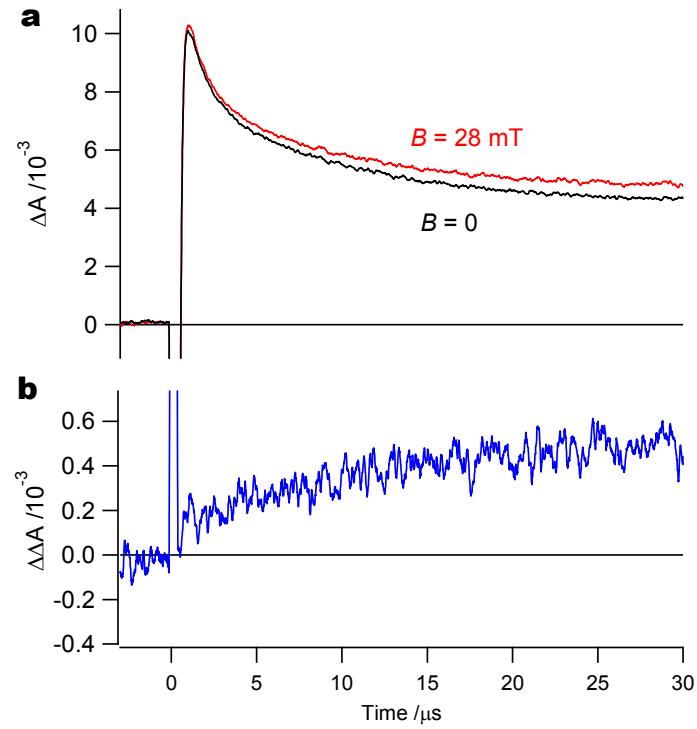


**Fig. S8.** Transient absorption kinetic time profiles of the intermolecular photochemical reaction of  $\sim 110$   $\mu M$  FAD with the apo form of  $\sim 110$   $\mu M$  garden warbler cryptochrome-1a, at 270 K, in  $\sim 50\%$  glycerol solution, 20 mM HEPES buffer, 500 mM NaCl, pH 7.4. **(a)** Kinetic traces with and without a 28 mT magnetic field after 100 ns boxcar smoothing. **(b)** Difference signals calculated from the data in (a):  $\Delta \Delta A = \Delta A(28 \text{ mT}) - \Delta A(0)$ . The excited *triplet* state of the flavin undergoes electron transfer reactions with unknown solvent-exposed tryptophan and/or tyrosine residues on the surface of the protein.

**3. Correlation between the magnetic field effect on the yield of RP2 and the lifetime of RP1 in *Ec*PL.**

**Table S1.** *Ec*PL data plotted in Fig. 5

25% glycerol		
$T / \text{K}$	$\tau / \mu\text{s}$	$ MFE  / \%$
265	1.7	$5.5 \pm 0.9$
270	1.3	$1.9 \pm 0.5$
275	1.6	$2.8 \pm 0.9$

50% glycerol		
$T / \text{K}$	$\tau / \mu\text{s}$	$ MFE  / \%$
235	7.4	$14.0 \pm 2.5$
240	7.5	$13.3 \pm 2.2$
	6.0	$11.2 \pm 1.4$
245	6.6	$9.9 \pm 1.8$
250	5.4	$7.5 \pm 1.9$
	4.8	$10.7 \pm 1.0$
255	4.6	$9.6 \pm 1.6$
260	3.6	$6.8 \pm 1.1$
	3.2	$5.4 \pm 0.7$
265	3.1	$6.6 \pm 2.0$
270	2.3	$5.4 \pm 1.4$
	2.1	$5.1 \pm 0.6$

65% glycerol		
$T / \text{K}$	$\tau / \mu\text{s}$	$ MFE  / \%$
250	5.7	$9.4 \pm 1.6$
260	4.6	$10.4 \pm 1.2$
270	4.3	$9.7 \pm 2.1$

$\tau$  is the lifetime of RP1 (measured at 600 nm) and  $|MFE|$  is the absolute value of the magnetic field effect (measured at 510 nm) on the yield of RP2.

#### 4. Calculation of $B_{1/2}$

Values of  $B_{1/2}$  were calculated using the Weller equation (6):

$$B_{1/2} = \sqrt{3} \frac{\tilde{a}_A^2 + \tilde{a}_B^2}{\tilde{a}_A + \tilde{a}_B} \quad (1)$$

where A and B label the radicals and  $\tilde{a}_K$  is the effective hyperfine coupling (HFC) of radical K, given by (7):

$$\tilde{a}_K = \sqrt{\frac{4}{3} \sum_i a_{iK}^2 I_{iK} (I_{iK} + 1)}. \quad (2)$$

$a_{iK}$  and  $I_{iK}$  are the isotropic HFC and the spin quantum number of nucleus  $i$  in radical  $K^*$ . Isotropic HFCs (Table S2) were calculated (by I. Kuprov) with Gaussian 03 using the UB3LYP/EPR-III level of theory. Lumiflavin was used as a proxy for FAD.

**Table S2.** Isotropic HFCs of  $\text{FAD}^{\bullet-}$  and  $\text{TrpH}^{\bullet+}$

$\text{FAD}^{\bullet-}$		$\text{TrpH}^{\bullet+}$	
	HFC / $\mu\text{T}$		HFC / $\mu\text{T}$
N5	523.3	N6	146.5
N6	188.7	N9	321.5
N14	-3.5	H16	-39.6
N16	-38.3	H17	-93.1
H20	56.5	H18	1604.6
H21 <sup>a</sup>	-141.6	H19	45.7
H22 <sup>a</sup>	-141.6	H20	-10.4
H23 <sup>a</sup>	-141.6	H21	23.3
H24	-387.2	H22	-278.0
H25 <sup>b</sup>	439.9	H23	-598.3
H26 <sup>b</sup>	439.9	H24	-488.0
H27 <sup>b</sup>	439.9	H25	-363.7
H28 <sup>c</sup>	0.0	H26	-208.3
H29 <sup>c</sup>	407.0	H27	-40.0
H30 <sup>c</sup>	407.0		
H31	-18.9		

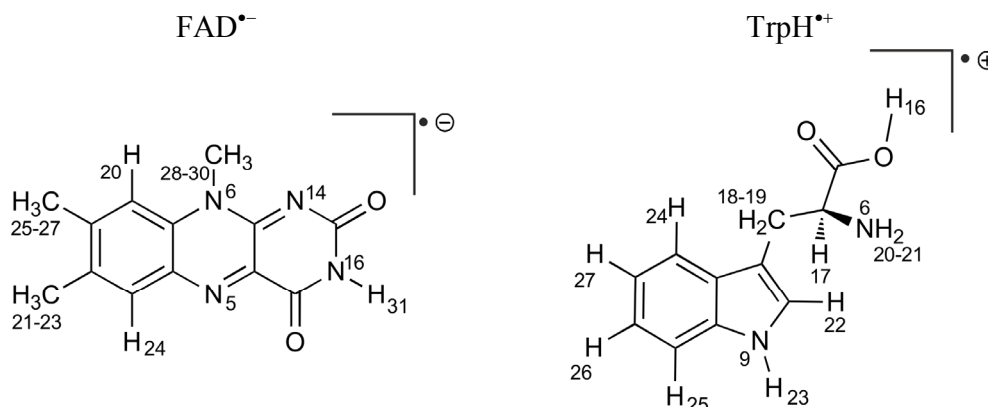
\* The literature has conflicting definitions of the effective hyperfine coupling constant. We have chosen to use a definition incorporating a factor of 4/3 (Rodgers *et al.* *J. Am. Chem. Soc.* **129**, 6746-6755 (2007)). The version of Equation (1) given by Weller *et al.* has a leading factor of 2 instead of  $\sqrt{3}$  because their version of Equation (2) does not contain the 4/3 factor.

<sup>a</sup> Average of values for H21, H22 and H23 to allow for internal rotation of methyl group.

<sup>b</sup> Average of values for H25, H26 and H27 to allow for internal rotation of methyl group.

<sup>c</sup> H29 and H30 represent the protons of the first methylene group of the ribityl chain in FAD. The HFC of H28 (9.9  $\mu$ T) was set to zero.

The atom numbers in Table S2 are those assigned by the Gaussian calculation (see below)



Using the data in Table S2, Equations (1) and (2) give  $\tilde{a}_{\text{FAD}} = 1.40$  mT and  $\tilde{a}_{\text{Trp}} = 1.94$  mT and hence  $B_{1/2} = 2.97$  mT.

Rodgers *et al.* have investigated the accuracy of Equation (1) using the exponential model (8, 9) in which radical pairs are assumed to recombine from the singlet and triplet states with the same rate constant,  $k$  (10). When  $k \ll \tilde{a}_K$  ( $K = A, B$ ), Equation (1) was found to give an upper bound to the ‘true’ value of  $B_{1/2}$  (determined by simulating the magnetic field dependence of the product yields). When  $k \approx \tilde{a}_K$ , Equation (1) gives a good estimate of the ‘true’ value, and when  $k \gg \tilde{a}_K$ , it dramatically underestimates  $B_{1/2}$ . From the values of  $k_f$  and  $k_b$  reported in the text ( $1\text{--}5 \times 10^5 \text{ s}^{-1}$ ) and the values of  $\tilde{a}_K$  quoted above (N.B.  $1 \text{ mT} \approx 1.76 \times 10^8 \text{ rad s}^{-1}$ ), it is clear that  $k \ll \tilde{a}_K$ . The ‘true’ value of  $B_{1/2}$  should therefore be smaller than the Weller value of  $\sim 3$  mT. The experimental observation that  $B_{1/2} \approx 10\text{--}12$  mT therefore strongly suggests the involvement of additional processes that broaden the magnetic field-dependence of the reaction yield.



## 5. Simulation of magnetic field effects

The magnetic field effects shown in Fig. 6 were calculated using the equation of motion of the radical pair spin density operator  $|\rho(t)\rangle$  in Liouville space:

$$\frac{d|\rho(t)\rangle}{dt} = \left( -i\hat{H} + \hat{K} + \hat{R} \right) |\rho(t)\rangle \quad (3)$$

The coherent and incoherent spin dynamics resulting from Zeeman and hyperfine interactions, chemical reactivity, and decoherence/relaxation processes were included by means of the superoperators  $\hat{H}$ ,  $\hat{K}$ , and  $\hat{R}$  respectively.

The quantum yield of RP2 ( $\Phi_{\text{RP2}}$ ) was determined from Equation (3) using the *Spinach* spin dynamics package (11) with spin relaxation added as summarized below. *Spinach*'s zero-track elimination (ZTE) routine was used to reduce the dimension of the Liouvillian (12). A non-linear least squares fitting procedure (the *lsqnonlin.m* routine from the *Optimisation Toolbox* in MATLAB 2010b) was used to fit the calculated field-dependence of  $\Phi_{\text{RP2}}$  to the experimental data. The background field experienced by the sample when no current flowed in the Helmholtz coils was assumed to be negligible.

**Hamiltonian superoperator,  $\hat{H}$ .** The electron Zeeman interactions of the two radicals were assumed to be isotropic with identical  $g$ -values ( $g = 2$ ). At the weak fields considered here, any effects of different  $g$ -values or of nuclear Zeeman interactions are negligibly small. It proved computationally impracticable to include more than 5 nuclear spins in the calculation (one  $^{14}\text{N}$  and four  $^1\text{H}$  with isotropic HFCs, giving a Liouvillian matrix with dimension 36,864 prior to ZTE and 6,930 after ZTE). The two largest HFCs in  $\text{TrpH}^{\bullet+}$  and the largest in  $\text{FAD}^{\bullet-}$  were included explicitly. The remaining HFCs in each radical were lumped together into a single spin-1/2 nucleus with an isotropic HFC ( $a'$ ) adjusted so that the correct value of  $\tilde{a}_{\text{K}}$  was obtained from Equation (2), see Table S3. The same HFCs were used for both proteins.

**Table S3.** HFCs used to calculate magnetic field effects

FAD <sup>•−</sup>		TrpH <sup>•+</sup>	
	HFC / $\mu\text{T}$		HFC / $\mu\text{T}$
N5	523.3	H18	1604.6
$a'$	1106.5	H23	−598.3
		$a'$	915.7

**Kinetic superoperator,  $\hat{K}$ .** The calculation was based on the reaction scheme in Fig. 4, ignoring the slow reactions that return RP2 to the ground state and assuming that RP1 is formed instantaneously at  $t = 0$  in a pure singlet state. Spin-selective electron–hole recombination of the singlet radical pair (rate constant  $k_b$ ) and spin-independent formation of RP2 from RP1 (rate constant  $k_f$ ) were included by means of Haberkorn recombination operators unless otherwise stated (13).

**Relaxation superoperator,  $\hat{R}$ .** Initial simulations were performed to investigate the magnetic responses of the  $[\text{FAD}^{\bullet-} \text{TrpH}^{\bullet+}]$  radical pair in the absence of relaxation processes.  $k_f$  was fixed at  $2.5 \times 10^5 \text{ s}^{-1}$  (as described in the text),  $k_b$  was varied to cover the range  $0.5 \leq k_b / k_f \leq 6$ , and the quantum yield of RP2,  $\Phi_{\text{RP2}}(B)$ , was determined for magnetic fields,  $B$ , in the range  $0 < B < 50 \text{ mT}$ . The percentage low and high field effects (LFE and HFE) were calculated as

$$\frac{\max[\Phi_{\text{RP2}}(B)] - \Phi_{\text{RP2}}(0)}{\Phi_{\text{RP2}}(0)} \times 100\% \quad \text{and} \quad \frac{\Phi_{\text{RP2}}(0) - \Phi_{\text{RP2}}(50 \text{ mT})}{\Phi_{\text{RP2}}(0)} \times 100\% \quad (4)$$

respectively, with the results shown in Fig. S9.

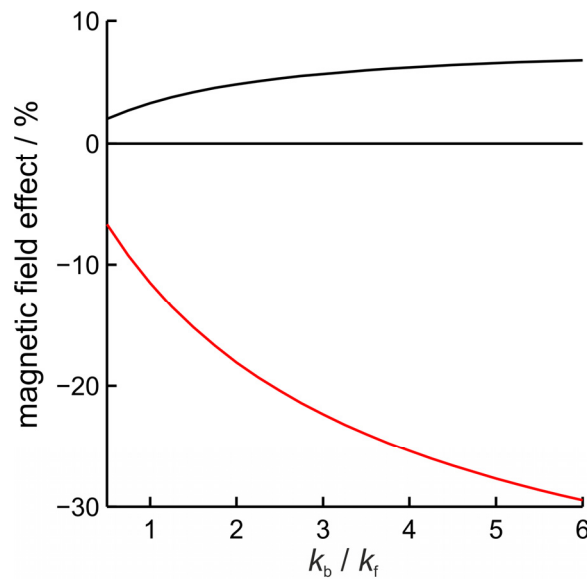


**Fig. S9.** Dependence on  $k_b / k_f$  of the calculated percentage LFE (black) and HFE (red) magnetic field effects for  $[\text{FAD}^{\bullet-} \text{TrpH}^{\bullet+}]$  with  $k_f = 2.5 \times 10^5 \text{ s}^{-1}$ ,  $k_{\text{STD}} = 0$ .

These simulations indicate that the percentage magnetic field effect for the reaction scheme in Fig. 4 increases monotonically with  $k_b / k_f$ . The estimated values of  $k_b / k_f$  obtained for AtCry ( $\sim 2.0$ ) and EcPL ( $\sim 0.5$ ) suggest a possible rationale for the larger magnetic response for AtCry (Fig. 6). Fig. S9 may also be used to rationalise the correlation between the magnetic field effect on EcPL and the RP1 lifetime (Fig. 5). As the temperature is lowered and/or the glycerol content is increased,  $k_f$  decreases causing  $k_b / k_f$  to increase, predicting a larger magnetic response.

Attempts to fit the data in Fig. 6 without relaxation were not successful (Fig. S10).  $k_f$  was fixed at  $2.5 \times 10^5 \text{ s}^{-1}$  (see text) and  $k_b$  was the only variable parameter. The values of  $k_b$  returned by the fitting procedure were  $3.8 \times 10^5 \text{ s}^{-1}$  (AtCry) and  $9.1 \times 10^4 \text{ s}^{-1}$  (EcPL). Of the various relaxation/decoherence models summarized below, only singlet–triplet dephasing provided a satisfactory description of the data in Fig. 6.

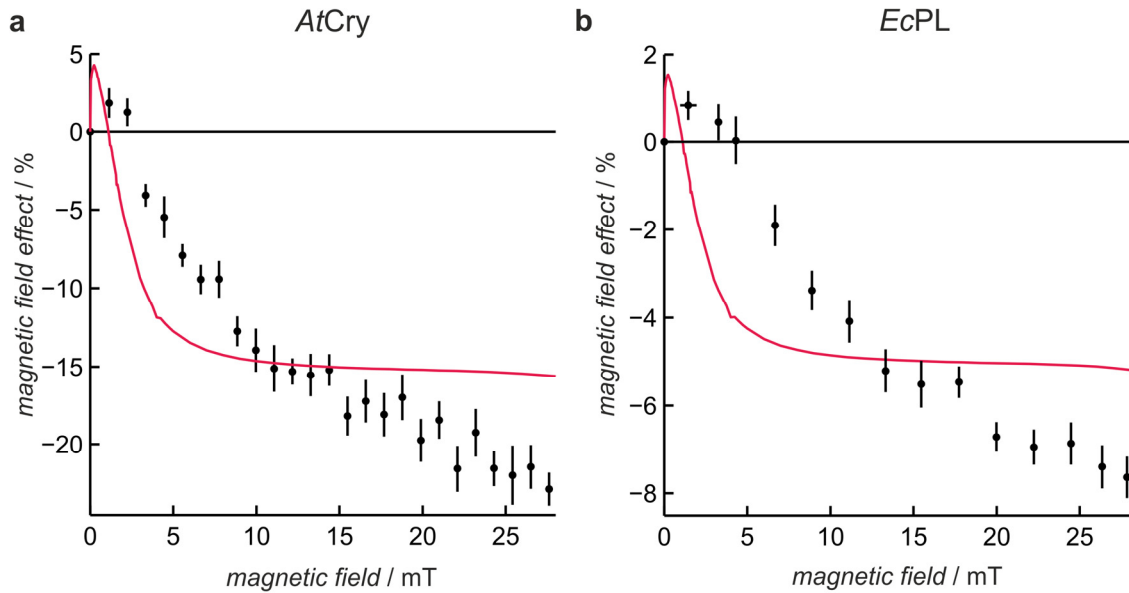


**Fig. S10.** The results of attempts to fit the data of Fig. 6 without including spin relaxation. (a) AtCry. (b) EcPL.

**Singlet–triplet dephasing** was included by means of the phenomenological superoperator (14)

$$\hat{R} = -k_{\text{STD}} \sum_{q=0,\pm 1} \{ |ST_q\rangle\langle ST_q| + |T_qS\rangle\langle T_qS| \} \quad (5)$$

The results are described in the text. Agreements with the data (Fig. 6) of comparable quality were obtained with the three rate constants  $k_b$ ,  $k_f$ , and  $k_{\text{STD}}$  scaled identically. Fixing the value of  $k_f$  as described in the text allowed a unique fit.

**Modulation of anisotropic HFCs.** Spin relaxation arising from modulation of anisotropic HFCs by isotropic rotational diffusion was included by means of Redfield theory (15, 16). The optimization variables were  $k_b$ ,  $k_f$  and the rotational correlation time,  $\tau_c$ . Restrictions on CPU time limited the calculation to three anisotropic HFCs (Table S4: Gaussian 03, UB3LYP/EPR-III), chosen for their large isotropic and anisotropic couplings.

**Table S4.** Selected anisotropic HFCs of FAD $^{\bullet-}$  and TrpH $^{\bullet+}$

		$A_{jj} / \mu\text{T}$	Principal axes <sup>a</sup>		
FAD $^{\bullet-}$	N5	-100.1	0.9581	-0.3068	0.0000
		-86.8	0.3068	0.9518	0.0000
		1756.9	0.0000	0.0000	1.0000
	H25	610.6	0.6882	0.0517	0.7237
		612.5	0.6968	-0.3254	-0.6393
		724.8	0.2024	0.9442	-0.2600
TrpH $^{\bullet+}$	H23	-1082.6	0.7540	0.6139	-0.2336
		-705.4	0.2344	0.0808	0.9688
		-6.9	-0.6136	0.7852	0.0830

<sup>a</sup>In the coordinate system used in the Gaussian output log file. Same atom numbering as in Table S2.

**Phenomenological exponential relaxation** was modelled as described by Bagryansky *et al.* (17) using time constants  $T_0$  at zero-field, and  $T_1$  and  $T_2$  at high field. Both field-independent and field-dependent  $T_1$  and  $T_2$  parameters were investigated. In the latter case, the relaxation rate varied with the strength of the applied magnetic field,  $\omega_0 = \gamma_e B_0$ , and an adjustable correlation time,  $\tau_c$ , as  $\tau_c / (1 + \omega_0^2 \tau_c^2)$ .

**Lindblad master equation.** Following Gauger *et al.* (18), relaxation induced by randomly fluctuating fields in three orthogonal directions was modelled using the Lindblad approach. The relaxation rates were assumed to have the form  $\tau_c / (1 + \omega_0^2 \tau_c^2)$  where the correlation time  $\tau_c$  was treated as a variable parameter.

**Jones-Hore kinetic superoperator.** The recently proposed alternative to the Haberkorn treatment of spin-selective recombination kinetics (13), which produces twice the singlet–triplet dephasing, was incorporated as described by Jones and Hore (19).



**Averaging of anisotropic hyperfine interactions.** Rotational diffusion in the viscous solutions used to obtain the data in Fig. 6 may not be sufficiently fast to average completely the anisotropic HFCs. Simulations were therefore performed without added relaxation, with spherical averaging over uniform distributions of radical pair orientations, using the HFC tensors in Table S4.

**Various combinations of the above approaches** were also explored.

## References

1. Henbest KB, *et al.* (2008) Magnetic-field effect on the photoactivation reaction of *Escherichia coli* DNA photolyase. *Proc. Natl. Acad. Sci. USA* 105:14395-14399.
2. Weber S, *et al.* (2010) Origin of light-induced spin-correlated radical pairs in cryptochrome. *J. Phys. Chem. B* 114:14745-14754.
3. Biskup T, *et al.* (2011) Time-resolved EPR identifies unexpected electron transfer in cryptochrome. *Angew. Chem. Int. Ed.*:in press.
4. Miura T, Maeda K, Arai T (2003) Effect of coulomb interaction on the dynamics of the radical pair in the system of flavin mononucleotide and hen egg-white lysozyme (HEWL) studied by a magnetic field effect. *J. Phys. Chem. B* 107:6474-6478.
5. Hore PJ, Kaptein R (1983) Proton nuclear magnetic-resonance assignments and surface accessibility of tryptophan residues in lysozyme using photochemically induced dynamic nuclear-polarization spectroscopy. *Biochemistry* 22:1906-1911.
6. Weller A, Nolting F, Staerk H (1983) A quantitative interpretation of the magnetic-field effect on hyperfine-coupling-induced triplet formation from radical ion-pairs. *Chem. Phys. Lett.* 96:24-27.
7. Schulten K, Bittl R (1986) Probing the dynamics of a polymer with paramagnetic end groups by magnetic-fields. *J. Chem. Phys.* 84:5155-5161.
8. Brocklehurst B (1976) Spin correlation in geminate recombination of radical ions in hydrocarbons. 1. Theory of magnetic-field effect. *J. Chem. Soc. Faraday Trans. II* 72:1869-1884.
9. Kaptein R, Oosterhoff JL (1969) Chemically induced dynamic nuclear polarization II: (relation with anomalous ESR spectra). *Chem. Phys. Lett.* 4:195-197.
10. Rodgers CT, Norman SA, Henbest KB, Timmel CR, Hore PJ (2007) Determination of radical re-encounter probability distributions from magnetic field effects on reaction yields. *J. Am. Chem. Soc.* 129:6746-6755.
11. Hogben HJ, Krzystyniak M, Charnock GTP, Hore PJ, Kuprov I (2011) *Spinach* - a software library for simulation of spin dynamics in large spin systems. *J. Magn. Reson.* 208:179-194.
12. Kuprov I (2008) Polynomially scaling spin dynamics II: Further state-space compression using Krylov subspace techniques and zero track elimination. *J. Magn. Reson.* 195:45-51.

13. Haberkorn R (1976) Density matrix description of spin-selective radical pair reactions. *Mol. Phys.* 32:1491-1493.
14. Shushin AI (1991) The effect of the spin exchange interaction on SNP and RYDMR spectra of geminate radical pairs. *Chem. Phys. Lett.* 181:274-278.
15. Goldman M (2001) Formal theory of spin-lattice relaxation. *J. Magn. Reson.* 149:160-187.
16. Kuprov I (2011) Diagonalization-free implementation of spin relaxation theory for large spin systems. *J. Magn. Reson.* 209:31-38.
17. Bagryansky VA, Borovkov VI, Molin YN (2007) Quantum beats in radical pairs. *Russ. Chem. Rev.* 76:493-506.
18. Gauger EM, Rieper E, Morton JLL, Benjamin SC, Vedral V (2011) Sustained quantum coherence and entanglement in the avian compass. *Phys. Rev. Lett.* 106:040503.
19. Jones JA, Hore PJ (2010) Spin-selective reactions of radical pairs act as quantum measurements *Chem. Phys. Lett.* 488:90-93.